Thermal and transport properties of the cubic semimetal $Y_3Ir_4Ge_{13}$: on the metallic border of thermoelectric merit

2007 J. Phys.: Condens. Matter 19 386205

(http://iopscience.iop.org/0953-8984/19/38/386205)

IOP PUBLISHING JOURNAL OF PHYSICS: CONDENSED MATTER

J. Phys.: Condens. Matter **19** (2007) 386205 (15pp) doi:10.1088/0953-8984/19/38/386205

Thermal and transport properties of the cubic semimetal $Y_3Ir_4Ge_{13}$: on the metallic border of thermoelectric merit

A M Strydom

Physics Department, University of Johannesburg, PO Box 524, Auckland Park 2006, South Africa

E-mail: amstrydom@uj.ac.za

Received 2 July 2007, in final form 30 July 2007
Published 29 August 2007
Online at stacks.iop.org/JPhysCM/19/386205

Abstract

The first results of thermal and electronic transport measurements on the cubic intermetallic compound $Y_3Ir_4Ge_{13}$ are reported. The electrical resistivity as well as the Hall coefficient show semimetallic activation behaviour. The specific heat is metallic-like at low temperatures. Towards higher temperatures the specific heat favours a description in terms of a Debye model together with Einstein modes that are attributable to details of the crystal structure of $Y_3Ir_4Ge_{13}$. The heat conductivity is surprisingly low, only weakly temperature dependent, and predominantly from phonons. A large thermoelectric power, 38 μV K^{-1}, is obtained at room temperature. The properties of $Y_3Ir_4Ge_{13}$ are discussed and compared with thermoelectric materials of current interest.

(Some figures in this article are in colour only in the electronic version)

1. Introduction

The family of ternary intermetallic compounds of composition $R_3T_4X_{13}$, originally designated as $RT_{1.1}M_{3.6}$ (R = rare-earth element, T = 3d, 4d, or 5d transition-block element, X = p-electron element) have been shown to be amenable to a wide variety of combinational possibilities. Two major groups consist of the stannides $R_3T_4Sn_{13}$ [1] and germanides $R_3T_4Ge_{13}$ [2], while compounds involving elements as diverse as Ca, Sr, and Th [3] and U [4] in the place of the R atom, as well as the indide $Ce_3Pt_4In_{13}$ [5] have also been reported. Interest in the physical properties of the $R_3T_4Sn_{13}$ class of compounds was initially driven by the discovery of superconductivity in a series of compounds involving only metallic elements, notably $Er_3Rh_4Sn_{13}$ in which the question of re-entrant superconductivity has been a matter of some debate [1, 6]. The T = Rh stannides with R = Yb [7] or the alkaline-earth element Ca [8], and the T = Ru germanides with R = Y or Lu [9] have also been investigated as compounds of unconventional superconductivity. In subsequent work a number of magnetic properties have been reported in $R_3T_4Sn_{13}$ systems. The rare-earth based Ir compounds order

magnetically between 0.6 and 50 K [10, 11]. Recent investigations have elucidated aspects of the heavy-fermion character of the Ce based stannides with T = Ir and Co [12, 13]. Similarly high values of the coefficient of electronic heat capacity (Sommerfeld coefficient), pointing to large effective electron masses or, alternatively, a large electronic density of states at the Fermi energy, were also found in the germanide $Ce_3Ru_4Ge_{13}$ [14]. The behaviour of the electrical resistivity in single-crystalline $Ce_3Co_4Sn_{13}$ is interpreted [15] in terms of a combination of semiconductor-like and Kondo properties in this compound.

The detailed description of the crystal structure in this class of compounds has received considerable interest. The in-depth crystallographic analysis of Miraglia *et al* [3] suggested the co-formation of a small component of a crystallographic superstructure in $R_3T_4X_{13}$ compounds where light rare-earth elements (R = La to Gd) are involved, on the basis of a doubling of the cubic lattice parameter of the $Pm3n$ space group. Associated with this superstructure is the possibility of site disorder between the Sn1 atoms in the crystallographic 2a position at (0, 0, 0), and the R atoms located at the 6d position, $(\frac{1}{4}, \frac{1}{2}, 0)$. A similar observation of Sn1 and R atomic site disorder was concluded from electron micrograph studies on the light rare-earth compounds [16]. An investigation on the two stannides $Ce_3Rh_4Sn_{13}$ and $Ce_3Ir_4Sn_{13}$ [17] showed, in contrast, ordered occupancies on the Ce, Rh(Ir) and Sn2 sites (Sn2 atoms located at $(x, y, 0)$ on the $24k$ sites), but a defect occupancy instead on the Sn1 site to the extent that, in for example the Rh compound, this Sn1 site suffers from an estimated 8% vacancy rate. Smaller deviations from full occupations on the R and Sn1 sites were also reported for the $Yb_3Rh_4Sn_{13}$ compound [18]. In the definitive work of Bordet *et al* [19] using synchrotron x-ray powder diffraction to study the crystallography of $La_3Rh_4Sn_{13}$, a doubling of the cubic lattice parameter, to $a_0 = 19.492$ Å, was reported to follow from a distortion of the Sn1–Sn2 filled cage. Interestingly, structural analyses on single-crystal material of $Ce_3Co_4Sn_{13}$ [15] revealed a *fully ordered* crystal structure of this compound with, in particular, none of the pathological partial site vacancy on the Sn1-2a(0, 0, 0) site as found in some of the isostructural compounds. The structurally ordered state in the Co derivatives was recently shown to occur in a series of $R_3Co_4Sn_{13}$ compounds with R = Pr, Nd, Sm, Gd, and Tb [20].

In this paper, findings of the first exploratory studies of the physical properties of the compound $Y_3Ir_4Ge_{13}$ are reported. The existence of $Y_3Ir_4Ge_{13}$ was published in the work of Venturini *et al* [2], but to the knowledge of the author no physical properties have been reported on it thus far. Interest stems here from the caged structure found in the $R_3T_4X_{13}$ class of compounds in which there are three 12-coordination cages, two of which house the Ge1 atoms and the R atoms respectively, and the third which is centred on the empty 6b$(\frac{1}{2}, \frac{1}{2}, 0)$ position (see figure 1). Cage structures of this nature provide interesting physical properties in their own right due to features that arise from the relatively large interatomic distances, but also due to the consequential possibilities to devise thermoelectric materials of high efficiency [21]. In this concept, an atom that is highly coordinated inside a large cage of neighbouring atoms could be expected to act as an effective scatterer of heat-carrying acoustic phonons through off-centre thermal motion ('rattling'). Three fundamental requirements for high thermoelectric efficiency are met when a state of suppressed thermal conduction occurs in a system with a good electrical conductivity as well as a high thermoelectric power.

2. Experimental details

Polycrystalline $Y_3Ir_4Ge_{13}$ material was prepared by arc melting stoichiometric quantities of the starting elements (purities in weight-%) Y (99.99), Ir (99.99), and Ge (99.9999). The resulting ingot was remelted several times in a slight underpressure of ultrahigh-purity argon to promote homogeneity. The weight loss upon melting was less than 0.5 wt%. The single-phase nature of

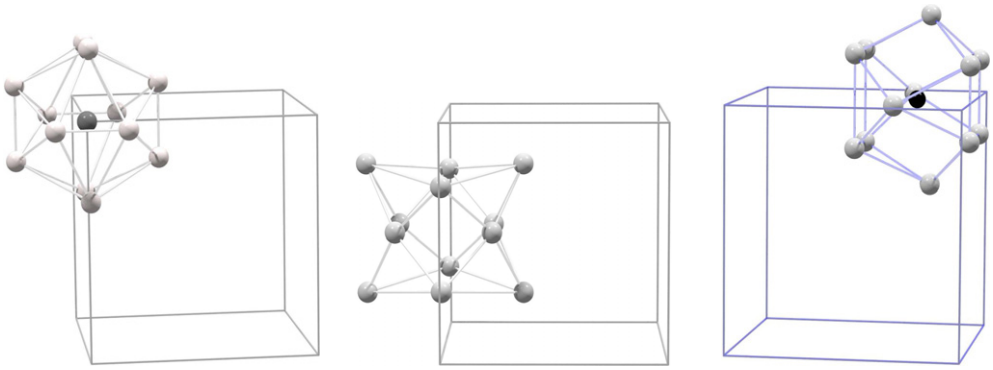

Figure 1. Cage formation in $Y_3Ir_4Ge_{13}$: cage centred on Ge1 (dark grey) located at 2a-(0 0 0) (left), cage centred on the empty 6b-($\frac{1}{2}$ $\frac{1}{2}$ 0) (middle), and cage centred on Y (black) located at 6d-($\frac{1}{4}$ $\frac{1}{2}$ 0) (right). The white spheres indicate Ge2 atoms.

the sample thus prepared was verified by powder x-ray diffraction on a *Philips PanAnalytical X'Pert Pro* instrument. The powder diffractogram showed a straightforward agreement with the expected $Pm3n$ body-centred cubic crystal structure. A few tiny diffraction lines not predicted by the $Pm3n$ space group were found to be eradicated by prolonged annealing (55 days at 1050 °C) of the as-cast sample ingot. These lines appear to originate from the stable hexagonal binary alloy Y_3Ge_5 [22]. A full-profile Rietveld refinement using *WinMProf* [23] on diffraction data of the annealed sample yielded a cubic lattice parameter of $a_0 = 8.945(5)$ Å, in close agreement with the previously reported value [2] of $a_0 = 8.948(6)$ Å. Heat treatment for the purpose of phase purification was similarly reported to have been applied to polycrystalline samples of $Y_3Co_4Ge_{13}$ [14].

A significant improvement in the refinement results could consistently be reached by setting the Ge1 and Ge2 atomic occupancy factors as variables in the refinement procedure. This resulted in the refinements converging on average to a $\simeq$4% vacancy in the Ge1 site at (0, 0, 0), which is significantly smaller than what was reported [17] for Sn1 vacancies in $Ce_3Rh_4Sn_{13}$ and $Ce_3Ir_4Sn_{13}$. The as-cast and annealed samples gave the same vacancy rates within the error of calculation, which means that the calculated Ge1 vacancy is not induced by the annealing process.

Samples were cut into geometries appropriate for various measurements by strain-free spark cutting. Aside from x-ray diffraction, all the measurements reported here were performed using a *Quantum Design Physical Properties Measurement System*[1].

3. Results

3.1. Specific heat

The specific heat, $C(T)$, of $Y_3Ir_4Ge_{13}$ is shown in the main panel of figure 2. The classical Dulong–Petit value of $3R$, in the case of $Y_3Ir_4Ge_{13}$ amounting to $C(T)/T = 1.663$ J/(mol f.u. K^2) at $T = 300$ K, closely predicts the room temperature specific heat (see inset (a) in figure 2). The electronic contribution to the specific heat is evaluated at low temperatures, as shown in figure 3(b). The Sommerfeld coefficient γ is calculated according to

[1] Quantum Design, Lusk Boulevard, San Diego, USA.

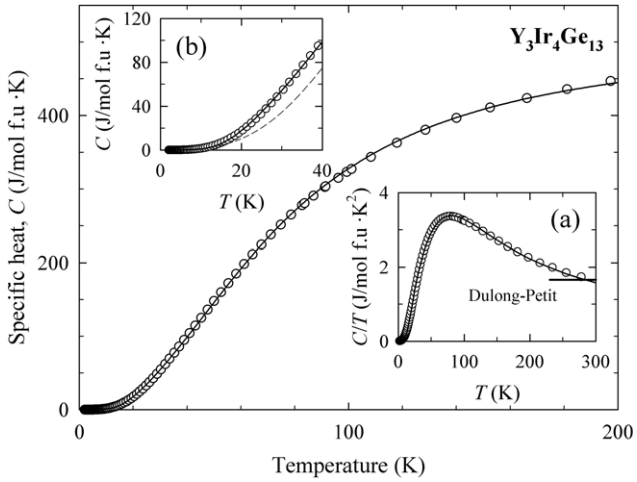

Figure 2. Specific heat of $Y_3Ir_4Ge_{13}$ over a wide range of temperature. The symbols are experimentally measured points. The solid lines in the main panel and those in both insets describe a fit incorporating 16 Debye characteristic modes ($\theta_D = 324$ K), plus one Einstein mode with $\theta_E = 342$ K and three further Einstein modes having $\theta_E = 110$ K. Inset (a) shows the specific heat in the form $C(T)/T$ up to room temperature. The room temperature value of $C(T)/T$ predicted by the Dulong–Petit law is shown by the horizontal marker in inset (a). Inset (b) shows, towards low temperatures, a comparison between a fit (dashed line) involving only acoustic modes from a total of 20 Debye atoms, according to equation (2), as well as a solid line fit depicting a Debye (equation (2)) and Einstein (equation (3)) multiplicity of modes as described for the fit in the main panel.

the relation

$$C(T)/T = \gamma + \beta T^2, \qquad \gamma = \frac{\pi^2}{2}\frac{N_A k_B^2}{\epsilon_F} \qquad \text{and} \qquad \beta = \frac{12\pi^4}{5} N_A k_B \frac{1}{\theta_D^3} \tag{1}$$

yielding $\gamma = 4.3(1)$ mJ (mol^{-1} K^{-2}) and $\beta = 0.89(1)$ mJ (mol^{-1} K^{-4}).

The resulting low-temperature estimate of the Debye temperature is $\theta_D^{LT} = 129.7$ K. However, no adjustment of the Debye temperature could describe the specific heat data in a satisfactory manner over a wide range of temperature within the Debye model,

$$C^D(T) = 9R\left(\frac{T}{\theta_D}\right)^3 \int_0^{\theta_D/T} \frac{x^4 e^x}{(e^x - 1)^2}\, dx. \tag{2}$$

This model yields the behaviour of a limited number of vibrational modes for a set of coupled oscillators. Instead, the solid line in figure 2 shows the result of a least-squares fit incorporating both Debye acoustic and Einstein optical vibrational modes in the total specific heat. Also included in this representation of the specific heat is the electronic contribution, calculated as described above ((1), figure 3(b)).

For N_E number of Einstein modes, the molar specific heat is given by:

$$C^E(T) = 3N_E R \frac{y^2 e^y}{(e^y - 1)^2}, \qquad y = \theta^E/T. \tag{3}$$

Iterated fits incorporating *both* types of modes, (2) and (3), were performed by fixing the respective number of Debye (n_D) and Einstein oscillators (n_E) for a particular fit, allowing both θ_D and θ_E to vary as fit parameters, and by subsequently noting the fit quality for various sets of (θ_D, θ_E). The solid-line fits shown in figure 2 reproduce the specific heat

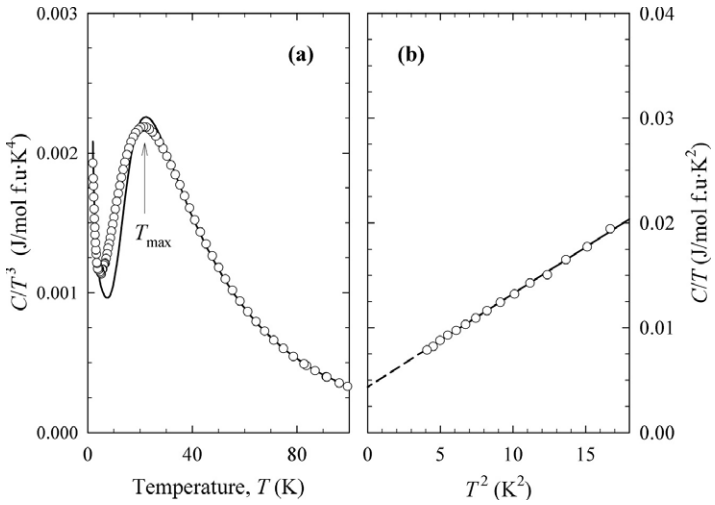

Figure 3. Specific heat of $Y_3Ir_4Ge_{13}$ at lower temperatures. Panel (a) shows the temperature dependence of the function $C(T)/T^3$. The local maximum, seen here at $T_{max} = 21$ K, substantiates the involvement of Einstein modes in the specific heat. This point is further supported by the theoretical description (solid (blue) line) of a fit incorporating both Einstein and Debye vibrational modes (cf figure 2). Panel (b) illustrates a plot of $C(T)/T$ against T^2 to facilitate calculation of the Sommerfeld coefficient, as explained in the text.

measured in $Y_3Ir_4Ge_{13}$ quite well over a wide range in temperature, and comprises *sixteen* Debye characteristic atoms with $\theta_D = 324(1)$ K, plus *one* Einstein characteristic atom with $\theta_E = 342(1)$ K and *three* further Einstein characteristic atoms with $\theta_E = 110(5)$ K. This multiplicity accounts for a total of 20 atoms per f.u. of $Y_3Ir_4Ge_{13}$. Figure 3(a) shows a plot of C/T^3 against T, a representation that is often used to assess the possible presence of low-frequency Einstein modes in the specific heat [24] through the occurrence of a maximum in $C(T)/T^3$ at $T = T_{max}$ when plotted in this way. The maximum, in this case at $T_{max} = 21$ K, could be interpreted as the temperature below which Einstein modes are frozen out. This is also the temperature where the deviation from a pure Debye description of the specific heat becomes conspicuous. It can be shown that $T_{max} \approx \theta_E/5$,[2] which is in good agreement with the above value obtained for the lowest-frequency Einstein vibrational mode of $\theta_E = 110(5)$ K.

The description of the specific heat in terms of a combination of acoustic and optic vibrational modes can readily be associated with the cage-like crystal structure of $Y_3Ir_4Ge_{13}$ (see figure 1). Four out of 20 atoms per f.u., namely 1 Ge1 atom and 3 Y atoms, are confined to two different cages built with Ge2 atoms. The Y atom, of which there are three per f.u., has an atomic mass 22% larger than that of Ge and can thus be expected to have a significantly lower natural frequency of oscillation. Yttrium is thus associated with the calculated Einstein temperature of 110(5) K of triple multiplicity, and the lighter Ge1 atom (one per f.u.) with the higher-frequency Einstein vibrational term of $\theta_E = 342(1)$ K.

Einstein-like modes of oscillations of the caged-up atoms would require them to execute off-centre thermal motions that are partly decoupled from that of the rest of the cage network of atoms. The Ge1–Ge2 interatomic distance in the first of the two cages is $d_{Ge1-Ge2} = 3.085$ Å, which exceeds the $d_{Ge-Ge} = 2.45$ Å distance in pure germanium by 25%. This situation is conducive to 'rattling' of the Ge1 atom within the twelvefold-coordinated Ge2 cage. The

[2] Ulrike Köhler (Max Planck Institute for Chemical Physics of Solids, Dresden, Germany) is thanked for pointing out this relation as a parallel to the $T_{max} \simeq \nu_E/3$ relation in terms of the Einstein frequency ν_E given in the work of [24].

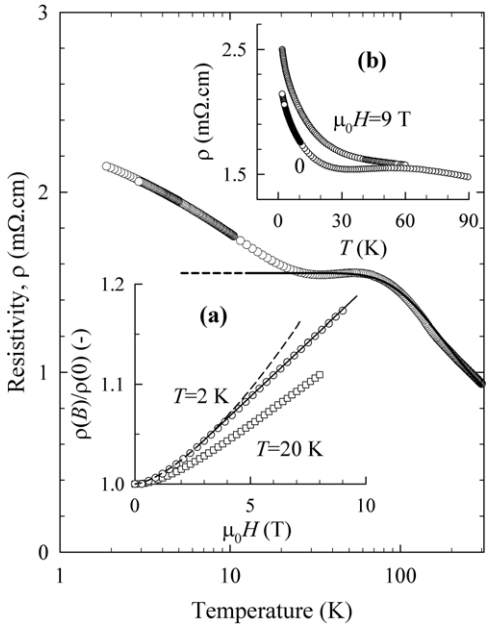

Figure 4. Electrical resistivity (ρ) of $Y_3Ir_4Ge_{13}$. The main panel shows $\rho(T)$ on semilog axes. The insets show the effect of an applied magnetic field; (a): $\rho(B)$ at two constant temperatures of 2 K and 20 K respectively, (b): $\rho(T)$ in zero field and in a constant field of 9 T. The dashed line in (a) shows the B^2 dependence of $\rho(T = 2\ \text{K})$ in low fields, and the solid line the B dependence in higher fields up to 9 T.

shortest Ge2–Ge2 distance between atoms making up the cage framework in $Y_3Ir_4Ge_{13}$ are, on the other hand, at a separation of $d_{\text{Ge2-Ge2}} = 2.683$ Å, which is only slightly larger but comparable to what is found in pure germanium. In the second cage, the Y atoms have 12 Ge2 atoms as nearest neighbours, see figure 1(c), situated at $d_{\text{Y-Ge2}} = 3.113$ Å. This may be compared to the sum of the covalent radii of Y and Ge, for which $r_{\text{Y}} + r_{\text{Ge}} = 2.84$ Å. Thus in this cage too the situation appears favourable for 'rattling' of the Y atoms.

In the isostructural two compounds $Ce_3Rh_4Sn_{13}$ and $Ce_3Ir_4Sn_{13}$ large atomic displacement factors were found for both the Sn1 and Sn2 atoms by means of crystallographic refinement calculations [17]. It is noted, however, that these two compounds suffered at the same time from a relatively large structural defect in the form of Sn1 vacancies (8% vacancy rate of Sn1 in $Ce_3Rh_4Sn_{13}$ and 24% of Sn1 in $Ce_3Ir_4Sn_{13}$). This might be ascribed to a tendency of Sn to evaporate during the arc melting process, a detrimental side-effect that is less likely to occur in the present germanide on account of the much higher melting point of elemental Ge.

3.2. Electrical resistivity and magnetoresistivity

Figure 4 illustrates the electrical resistivity (ρ) and magnetoresistance (MR) results on $Y_3Ir_4Ge_{13}$. The overall behaviour is not of a metallic character, with resistivity values of the order of a few mΩ cm and a two-step increase with decreasing temperature. Thus, apart from an intermediate plateau near 50 K, $\rho(T)$ has a negative slope over the whole investigated temperature range. Resistivity measurements on an as-cast sample yielded the same behaviour as that shown in figure 4.

A negative temperature coefficient of $\rho(T)$ was likewise found in two other isostructural stannide compounds, $Ce_3Ir_4Sn_{13}$ and $U_3Rh_4Sn_{13}$. In these two compounds the rise in ρ

with decreasing temperature is, in contrast to the present case of $Y_3Ir_4Ge_{13}$, likely due to incoherent Kondo scattering at high and intermediate temperatures that results from single-ion-type behaviour of the local cerium-derived 4f electron magnetic moment. The dc magnetic susceptibility of $Y_3Ir_4Ge_{13}$ (not shown) was measured and found to be diamagnetic, very small ($\simeq -8 \times 10^{-9}$ m^3/mol f.u.), and only very weakly temperature dependent, which confirms that scattering mechanisms with a magnetic origin can be excluded in the case of $Y_3Ir_4Ge_{13}$. A net diamagnetic susceptibility is associated with the measured diamagnetic signal that likely originates from the inner filled electron shells (closed orbits) dominating the Pauli paramagnetism from conduction electrons in the case of a low charge carrier density. Finally, it is of interest to note that in the related $R_3Ru_4Ge_{13}$ (R = Nd, Dy, Ho, Er, Yb, Lu, and Y) series of rare-earth based compounds, activated behaviour in the electrical resistivities was found [9] in all but $Yb_3Ru_4Ge_{13}$.

We take an empirical approach to describe the higher-temperature features of $\rho(T)$ in $Y_3Ir_4Ge_{13}$ by means of the expression:

$$\rho = \frac{\rho_0}{1 + \alpha \exp(-\Delta/2T)}. \tag{4}$$

The $\rho(T)$ data of $Y_3Ir_4Ge_{13}$ in figure 4 over one decade in temperature between 30 and 300 K are well described by (4) (see solid line in main panel of figure 4) using $\rho_0 = 1.550(25)$ mΩ cm for the saturation level, $\alpha = 2.0(1)$, and a temperature equivalent energy gap of $\Delta = 660(5)$ K. Equation (4) is a modified form of the standard activation behaviour: it incorporates an intermediate-temperature saturation level of the electrical resistivity to facilitate a description of the relaxing of the activation behaviour that is observed in $Y_3Ir_4Ge_{13}$ around 50 K. Three possible configurations in the energy bands could lead to this type of feature: (i) two successive energy gaps in the band structure, (ii) residual 'impurity' levels within an energy gap, the contribution to the electrical conductivity of which only becomes significant at temperatures T comparable to the energy k_BT of these levels, and (iii) a temperature-dependent energy gap, for instance when the energy gap is driven by temperature-dependent hybridization involving conduction electrons.

A resistivity behaviour qualitatively similar to that of $Y_3Ir_4Ge_{13}$ shown in figure 4 is also found in systems as diverse as the localized, magnetic d electron Kondo insulator FeSi [25] and the nonmagnetic semimetal ThPtSn [26]. The upturn in the low-temperature part of $\rho(T)$ does *not* conform to a variable-range hopping description of the form

$$\log \rho = \log \rho_0 \, (T_0/T)^{1/n}, \tag{5}$$

in which $n = 4$, for instance, is commonly associated with an electronic localization mechanism in a semiconductor with local disorder. Low-temperature inelastic scattering processes involve, in principle, both electron–electron and electron–phonon processes. The electron–phonon scattering events assist in electrons hopping between localized states without being activated across the band gap. The efficiency of phonon-assisted conductivity diminishes rapidly at low temperatures as phonons cease to be excited, hence an increase in resistivity at low temperatures. It is interesting to note that an applied field of 9 T (see inset (b) in figure 4) diminishes the $\simeq$50 K plateau, —behaviour which suggests that $\rho(T)$ in sufficiently large fields might end up displaying simple $\rho \sim \exp(\Delta/2T)$ activation behaviour. The magnetoresistance (MR) observed in $Y_3Ir_4Ge_{13}$ also argues against localization effects in this compound: a magnetic field would be expected to suppress the inelastic scattering processes that occur in such a case at low temperatures, yielding a reduced resistivity, i.e., a negative MR. The MR observed in $Y_3Ir_4Ge_{13}$ is, on the other hand, not only positive but even increases in magnitude as the temperature is lowered, see inset (a) in figure 4. It is therefore concluded that Coulomb interaction effects dominate the field-dependent electronic transport in $Y_3Ir_4Ge_{13}$.

Strong interaction effects in a d electron transition metal such as iridium could be brought about by a large d band spectral weight of the conduction electrons which, in iridium, would ordinarily be associated with electrons originating from the s atomic shell. The d band character of conduction electrons could in turn result from a Fermi level that is deep-seated within the d band or, on the other hand but possibly hand in hand with this phenomenon, a strong s–d band hybridization.

No saturation is evident in the transverse ($\mathbf{J} \perp \mathbf{B}$) magnetic field dependence of the resistivity of $Y_3Ir_4Ge_{13}$, as is shown in inset (a) of figure 4 for two isotherms. The MR is relatively large for a nonmagnetic system, namely $[\rho(B) - \rho(0)]/\rho(0) = 17\%$ at $T = 2$ K, $B = 9$ T. For fields up to 3 T, $\rho(B)/\rho(0)$ at $T = 2$ K follows a behaviour linear in B^2 as shown by the dashed line in figure 4(a). In larger fields, up to 9 T, the $\rho(B)/\rho(0)$, $T = 2$ K data follow a $\Delta\left[\rho(B)/\rho(0)\right] = aB$ dependence instead, which is illustrated by the solid line superimposed onto the 3 T $\leqslant B \leqslant$ 9 T data in figure 4(a). A magnetoresistance that is linear in B and also positive in sign is an electronic transport phenomenon that has received considerable interest over many years—see for instance the recent review by Abrikosov [27]. In a compensated metal (equal numbers of holes and electrons) with a simple Fermi surface composed of closed electron and hole sheets, semiclassical transport theory predicts that the MR should rather depend linearly on B^2. A small number of simple metals are known not to obey this prediction of MR (see [28] and references therein). In a recent discovery of similar behaviour in more complex materials, namely silver chalcogenides [29] it was shown that this pressure-tuned effect remarkably coincides with a change in the sign of the Hall coefficient, a scenario that has been predicted [30] when the conduction and valence bands touch or where the width of the energy gap in a semiconducting material approaches zero.

3.3. Hall coefficient

Measurements of the Hall coefficient could thus shed light on the influence of charge carrier density effects in the resistivity of $Y_3Ir_4Ge_{13}$, the Coulomb interaction mechanism that is evident from the above discussion, as well as on the possible scenario of a convergent valence band and conduction band in this material. The temperature dependence of the Hall coefficient R_H in $Y_3Ir_4Ge_{13}$ is shown in figure 5 on a semilog plot. An applied magnetic field of $B = 8$ T was used, in which the Hall resistance was verified to be a linear function of field. The values are overall positive and thus suggesting the importance of holes as charge carriers in $Y_3Ir_3Ge_{13}$. There is no change in the sign of R_H throughout the investigated temperature range, which argues against the application of the Abrikosov [30] theory of 'quantum magnetoresistance' and a linear energy spectrum for the magnetotransport in $Y_3Ir_4Ge_{13}$. While the possibility of a change in the sign of R_H at elevated temperatures cannot be excluded, the field-linear magnetoresistance in $Y_3Ir_4Ge_{13}$ appears to be limited to the low-temperature region and is not observed at temperatures above about 20 K.

The overall behaviour of $R_H(T)$ echoes that of the electrical resistivity $\rho(T)$. The magnitude of R_H shows a sixfold, $\Delta R_H \propto -\log T$ increase below room temperature, as shown by the guide-to-the-eye solid line in figure 5, down to 50 K where a plateau is reached at $R_H = 90(3) \times 10^{-10}$ m^3 C^{-1}. This translates into a charge carrier density of only $n_{50K} = 0.30(2)$ carriers/(f.u.) at the plateau, among the 20 atoms per f.u. in $Y_3Ir_4Ge_{13}$, assuming a one-band model. The single-band carrier concentration at room temperature amounts to approximately $n_{300K} = 1.5(8)$ carriers/(f.u.). A crude summation of the conduction electrons in $Y_3Ir_4Ge_{13}$ with 0.4 s conduction electrons per yttrium atom [31] plus 0.6 s conduction electrons per iridium atom [32], yields 3.6 conduction electrons per f.u.,—a value that is well in excess of the Hall-derived result.

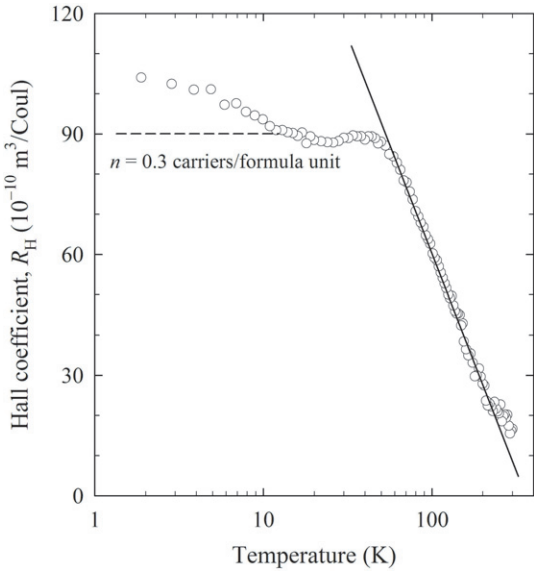

Figure 5. Temperature dependence of the Hall coefficient in a constant field of 8 T. The solid line on the data is a guide to the eye, and the horizontal dashed line indicates the calculated carrier concentration at the $T \simeq 50$ K plateau.

3.4. Thermal conductivity and thermoelectric power

The temperature dependence of the thermal transport in $Y_3Ir_4Ge_{13}$, including the thermal conductivity (main panel, log–log plot) and the thermoelectric effect (inset), are shown in figure 6. The total measured thermal conductivity κ_T is reduced by a factor of 10 upon cooling from room temperature to 2 K and shows a temperature dependence that is surprisingly weak for either a metal or a semimetal. We extract the electronic contribution κ_E to the total heat conductivity by means of the Wiedemann–Franz relation [33], for which the thermal conductivity is, in a highly degenerate electron gas, related to σ, the electrical conductivity:

$$L_0 = \frac{\kappa}{\sigma T}, \tag{6}$$

through the temperature-independent Lorenz number:

$$L_0 = \left(\frac{\pi k_B}{e\sqrt{3}}\right)^2 = 2.45 \times 10^{-8}\ \mathrm{W\ \Omega\ K^{-2}}. \tag{7}$$

The electrical conductivity $\sigma(T)$ and the thermal conductivity $\kappa(T)$ used in this expression, as well as the thermopower $S(T)$, were measured simultaneously and with the same set of contacts to the sample. The electronic part κ_E thus calculated (see figure 6) is 1–2 orders of magnitude *less* than the total measured thermal conductivity. The electrons in $Y_3Ir_4Ge_{13}$ are consequently not important heat carriers over the entire temperature range investigated, nor are they likely to act as an important scattering mechanism for other heat-carrying particles or quasiparticles.

In a general nonmagnetic semiconductor where electronic contributions to transport phenomena may be neglected, the kinetic theory-derived [33] conductivity of heat is given by:

$$\kappa = \tfrac{1}{3}\, C v_{ph} \ell \tag{8}$$

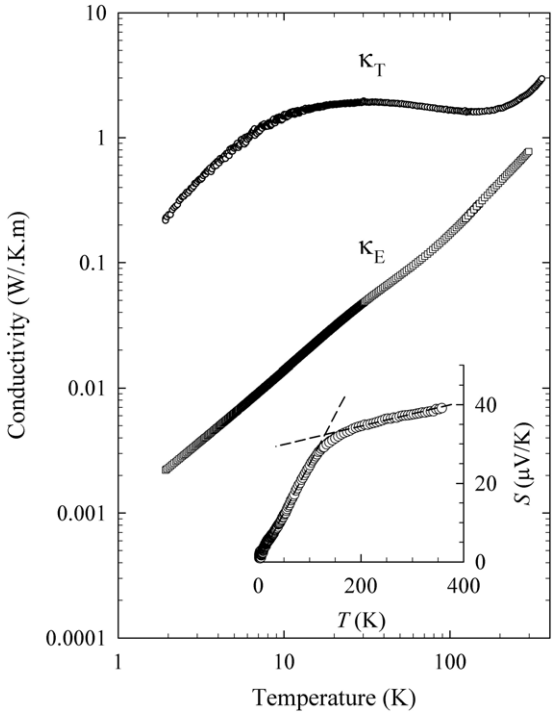

Figure 6. Temperature dependence of the total measured heat conductivity κ_T and the calculated electronic contribution κ_E on a log–log plot (main panel). Inset: Thermopower of $Y_3Ir_4Ge_{13}$. The guide-to-the-eye dashed lines emphasize the linear behaviour of $S(T)$ in two distinct regions.

in terms of the average quasiparticle (phonon) velocity v_{ph} and the mean free path length ℓ of the quasiparticle between collisions. In the remainder of the discussion, we approximate the (phononic) lattice thermal conductivity to $\kappa_L \simeq \kappa_T$, for simplicity and on strength of the above comparison between κ_E and κ_T. According to (8), $\kappa_L(T)$ would then assume the T^3 temperature dependence of the specific heat C at low temperatures. At the same time, the magnitude of κ_L may be limited by ℓ-related size effects such as grain boundaries, scattering from lattice imperfections and defects, and phonon–phonon scattering processes. Below the weak maximum near 20 K in the total thermal conductivity of $Y_3Ir_4Ge_{13}$, $\kappa_L(T)$ does not show unambiguous power-law behaviour, but the rate at which κ_L decreases is, in any event, much reduced from the T^3-related behaviour that would be expected if (8) was valid. This, together with the overall very low values of κ_L measured in $Y_3Ir_4Ge_{13}$, suggest the operation of an additional scattering mechanism(s) of the heat-carrying phonons.

Towards higher temperatures, the resistive U-processes (aside from phonon–phonon scattering in normal momentum-conserving N-processes) should lead to a T^{-1} dependence of κ_L at intermediate temperatures, for either metals or semimetals [34]. No such behaviour is evident in $\kappa_L(T) \simeq \kappa_T(T)$ in figure 6. This discrepancy cannot be ascribed to the influence of electronic thermal conduction: the calculated electronic contribution, $\kappa_E(T)$, is comparatively too small to be a driving factor in the total conduction of heat and to thus manipulate κ_T in $Y_3Ir_4Ge_{13}$ to any large extent.

A plateau in $\kappa_L(T)$, or a very weak temperature dependence of κ_L as is achieved in the present case upward of about 20 K, is often generically associated with a material of poor crystallinity. As will be shown below, the electronic part of the heat conductivity does not point

to the significance of lattice imperfections as such as a scattering mechanism in $Y_3Ir_4Ge_{13}$, and therefore only grain boundaries, as a size effect, are left to be considered as a defect-related factor limiting the conduction of heat by phonons in $Y_3Ir_4Ge_{13}$.

We consider next the effect of rattling atoms, the presence in $Y_3Ir_4Ge_{13}$ of which was implied in the analysis of the specific heat in section 3.1. Local anharmonic vibrations from 'rattling' atoms are known to be effective resonant scatterers for heat-carrying acoustic phonons [35]. A dip or plateau-like feature found in the (lattice) thermal conductivity of filled or partially filled skutterudites [36], around ∼20–200 K, and of the Eu based clathrate $Eu_8Ga_{16}Ge_{30}$ [35, 37], at ∼5–30 K, is attributed to heat-carrying phonons being scattered from the vibrations of host atoms in these two atomic cage classes of materials. The thermal conductivity in such a case is not only rendered flat and near temperature independent, simulating that of an amorphous material, but also severely reduced in magnitude. The overall magnitude of κ_L values obtained in $Y_3Ir_4Ge_{13}$ are comparable to those of the clathrates $Ba_8Ga_{16}Ge_{30}$ [38] and $Eu_8Ga_{16}Ge_{30}$ [35], as well as to those of skutterudite materials [36]. These materials are being studied extensively as they are considered amenable to the 'phonon-glass' approach to designing materials of high thermoelectric merit [21, 39–42].

In contrast to the phononic part, the electronic thermal conductivity $\kappa_E(T)$ of $Y_3Ir_4Ge_{13}$ does mirror its specific heat (see figure 3(b)) below about 20 K in that κ_E is practically linear in T. This is the prediction [33] for electrons in a Fermi gas,

$$\kappa_E(T) = \frac{\pi^2 n k_B^2 T \tau}{3m} \tag{9}$$

in terms of an electron concentration n and a time τ between collisions. Metallic behaviour, as opposed to semiconductor behaviour, is therefore plausible in $Y_3Ir_4Ge_{13}$. The very low values of electronic conduction of heat can be associated either with an effective scattering mechanism impeding the heat transport of electrons, or with a low electronic concentration in this material. Electron–phonon scattering could in principle be responsible for suppressing the electronic conduction at low temperatures, but effects of such a scattering mechanism are not evident in $\kappa_E(T)$ shown in figure 6. As is argued above, phononic transport itself in $Y_3Ir_4Ge_{13}$ is not overly efficient and is thus not *a priori* to be advanced as an important scattering mechanism for heat-carrying electrons. Finally, among defect-related factors, lattice imperfections of atomic dimensions could constrain the mean free path length related to electron transport [34],—the effects of which are also not seen in the $\kappa_E(T)$ data in figure 6. The near linear-in-T dependence of the calculated $\kappa_E(T)$ shown in figure 6 is of interest. We note that $\kappa_E(T)$ is overall a factor of 10 smaller but remarkably similar in its temperature dependence to the electronic heat conductivity reported on the α- and β-phases of the clathrate compound $Eu_8Ga_{16}Ge_{30}$ [37].

The thermopower $S(T)$ shown in the inset of figure 6 reaches a value of 38 μV K^{-1} at room temperature, which is intermediate between that of metals (∼1–10 μV K^{-1}) and semiconductors (∼10^2–10^3 μV K^{-1}). The thermopower is positive over the entire temperature range, which means that the charge carriers responsible for providing the thermal voltage must be hole dominated. Further evidence for the metallic disposition of $Y_3Ir_4Ge_{13}$ is furnished by comparing the thermopower predicted for a normal metal comprising a highly degenerate electron gas:

$$S_{\text{metal}}(T) = -\frac{\pi^2 k_B^2}{3|e|}\, T \left[\frac{1}{\sigma}\frac{\partial \sigma(\epsilon)}{\partial \epsilon}\right]_{\epsilon=\epsilon_F} \tag{10}$$

with that of a single-type carrier, non-degenerate semiconductor [43]:

$$S_{\text{semicond}}(T) = -\frac{k_B}{|e|}\left[\frac{(\epsilon_{cb} - \epsilon_F)}{k_B T} + \frac{1}{\tau(\epsilon)}\frac{\partial \tau(\epsilon)}{\partial \epsilon} + \frac{5}{2}\right] \tag{11}$$

(here $|e|$ is the electron charge, $\sigma(\epsilon)$ the energy-dependent electrical conductivity, ϵ_F the Fermi energy, ϵ_{cb} the conduction band-edge energy, and $\tau(\epsilon)$ the energy-dependent carrier relaxation time). The $S(T)$ data shown in the inset of figure 6 can, for the most part, be simulated by two regions of $S(T)$ tracing a linear-in-T dependence, (10), which implies a metallic character of the charge carriers involved in the thermopower of $Y_3Ir_4Ge_{13}$. The change in slope in the vicinity of 100 K may be ascribed to band restructuring or rearrangement in the electronic density of states, on which $S(T)$ is strongly dependent.

We take profit from the fact that the thermopower of $Y_3Ir_4Ge_{13}$ as well as its heat capacity, at low temperatures, are showing metallic behaviour, to modify the expression for the thermopower in (10) and in so doing to perform an alternative calculation of the carrier concentration in $Y_3Ir_4Ge_{13}$. For a free-electron gas, the relation between the density of states $\mathbb{N}(\epsilon_F)$ at the Fermi energy and the carrier concentration n, is $\mathbb{N}(\epsilon_F) = 3n/2\epsilon_F$. With the approximation of an energy-independent carrier relaxation time, at the low-temperature region under consideration, as well as a constant mean free path length for the thermal transport, (10) becomes [44]:

$$S = -\frac{\pi^2}{3}\frac{k_B^2}{|e|}\frac{3T}{2\epsilon_F}. \tag{12}$$

Comparing this expression with that of $\gamma = C_E T$ for the electronic specific heat as given in (1), leads to $C_E/S = ne$, whereby the thermopower probes the specific heat per electron [45] through a remarkably simple relation. A value of $n = 0.05$ carriers/(f.u.) is obtained for the present results of $Y_3Ir_4Ge_{13}$. This may be compared to the $T = 2$ K value of $n_{2K} = 0.2$ carriers/(f.u.) that is obtained by relating the Hall coefficient to the carrier concentration in a single-band approximation (see section 3.3). Although tenuous, the single-band approximation yielding $n_{2K} = 0.2$ carriers/f.u. nevertheless reflects an *upper limit* for the charge carrier density.

4. Discussion

The measurements reported here on $Y_3Ir_4Ge_{13}$ present an interesting variety of physical properties that range from good metallic behaviour to bordering on semimetallic behaviour. The admixture of such a variety of physical properties is a feature common to many intensively studied classes of materials, such as the strongly correlated electron systems. Thermoelectric materials that are currently attracting interest are, by design of one approach towards materials of higher efficiency, combinations of an amorphous (glass-like) phononic behaviour with crystal-like electronic transport [36].

The specific heat of $Y_3Ir_4Ge_{13}$ at the lowest temperature of this work (1.9 K) attests to behaviour that fits well with the free-electron or Fermi gas description, as does the calculated electronic component of the thermal conductivity, over a remarkably wide temperature range. The *temperature dependence* of the thermopower also reflects behaviour that is rather characteristic of a well-behaved metal. On the other hand, the sign of both the Hall coefficient and the thermopower suggest that electrical transport occurs in $Y_3Ir_4Ge_{13}$ predominantly by (higher mobility, or lighter mass) holes that are conceivably the result of (lower mobility, or heavier mass) electrons having been excited across an energy gap. A high effective electron mass is plausible when strongly hybridized bands are present, as is deduced from the magnetoresistance behaviour of $Y_3Ir_4Ge_{13}$. This picture is born out by the temperature dependence of the electrical resistivity that could be described by activation behaviour at temperatures near and below room temperature, but with an intermediate-temperature plateau possibly arising from in-gap levels. We cannot rule out the possibility that refinement of the

sample preparation procedure, measurement on single crystals, or even the use of starting elements of higher purities than what is used in this work (i.e. semiconductor grade elements), might eliminate the 'impurity' levels or confine them to lower temperatures.

It is of interest to consider distinguishing $Y_3Ir_4Ge_{13}$ as a low-carrier-concentration metal, or as a semimetal. One of the key issues of this paper is to have highlighted the ambivalent electronic character of this material, but further spectroscopic methods are called for to furnish complementary evidence in this regard. The electrical resistivity, the magnitude of the electronic heat conduction, and the Hall-derived charge carrier density value at low temperature all certainly favour a semimetallic description, but in the usual meaning of such a classification it remains to be verified whether $Y_3Ir_4Ge_{13}$ does in fact develop a zero-gap state (filled valence band gaplessly separated from the empty conduction band, with E_F at the juncture). An order-of-magnitude calculation of the mean free path length, $\ell = v_{th}\tau_{sc}$, in terms of the average thermal velocity $v_{th} = \sqrt{(3k_BT/m^*)}$ (m^* the charge carrier effective mass) and the scattering rate limited carrier lifetime $\tau_{sc} = m^*\mu/e$ ($\mu = 1/\rho ne$ is the Hall-derived carrier mobility) yields $\ell \simeq 10^{-10}$ m at $T = 20$ K. This value is of the order of interatomic distances in $Y_3Ir_4Ge_{13}$, which indicates that the system is situated at the border of metallicity and might well be approaching the metal–insulator transition at low temperatures. Although such a severely restricted mean free path length could originate from chemical (e.g. slight stoichiometry shifts) or metallurgical (e.g. microcracks) effects, it is difficult to reconcile either of these sources with the observed rise in resistivity below $T \simeq 20$ K. Alternatively though, this rise in resistivity might be traced to the freezing out of Einstein oscillator modes below 21 K (see figure 3) due to the possible 'lock-in' of rattling atoms into off-centre positions. On the other hand, the specific heat, the thermopower, and the charge carrier concentration obtained from these reflect metallic behaviour. It serves to be reminded, besides, that the measurement of these latter two physical properties suffers technically to a much lesser degree from sample metallurgical defects such as microcracks.

Supported by details of the crystal structure, the overall thermal conductivity as well as the higher-temperature specific heat of $Y_3Ir_4Ge_{13}$ lead to a compelling description of atomic 'rattling' or anharmonic vibrations of a small number of atoms that are more or less decoupled from the rest of the lattice, and yet influential enough to dominate these two physical properties. The dimensionless thermoelectric figure of merit is given by:

$$ZT = S^2\frac{T}{\rho\kappa}. \tag{13}$$

The data on $Y_3Ir_4Ge_{13}$ yield, at room temperature, $ZT = 0.02$. This value is of the same order of magnitude as, for instance, what is reached in clathrate compounds [37] at the much lower temperature of 100 K. A value of $ZT \geqslant 1$, regarded as the mark of a workable thermoelectric material, exceeds ZT of $Y_3Ir_4Ge_{13}$ by two orders of magnitude. While the thermal conductivity measured in $Y_3Ir_4Ge_{13}$ is comparable in magnitude with that of other contemporary materials of thermoelectric merit, efforts to improve ZT would have to deal with increasing the thermopower, without compromising the electrical conductivity. Such measures could include doping at appropriate energy levels or increasing the hole mobility to favour the thermopower over the electrical conductivity.

Intermetallic alloys are, by nature, prone to a variety of atomic and structural disorder. The presence of such disorder beyond the phase purification that was achieved in this exploratory work on $Y_3Ir_4Ge_{13}$, and its possible influence in certain physical properties reported here cannot be dismissed. It serves to point out, however, that the measured thermopower shows behaviour that reflects a remarkably simple band structure in this material.

The importance of atomic or crystallographic order/disorder should not be underestimated in materials deemed 'optimal' for thermoelectric applications. One of the presently highest-

merit room temperature thermoelectric materials is β-Zn_4Sb_3 [46], a material that is known to suffer from substantial disorder in the form of a number of glass-like Zn interstitial sites. A number of parallels may be drawn between β-Zn_4Sb_3 and $Y_3Ir_4Ge_{13}$: both materials are hole carrier (p-type) materials; as is the case with a number of other high-merit thermoelectric materials [46]. Both materials show diamagnetic behaviour [47]. The importance of a very low thermal conductivity *vis-à-vis* the need for a high thermopower, the latter which appears as a squared entity in the figure of merit (see (12)), is accentuated by the case of β-Zn_4Sb_3: it has a room temperature thermal conductivity at an extremely low 0.6 W K^{-1} m^{-1} (five times lower than that of $Y_3Ir_4Ge_{13}$), while the thermopower varies between 70 and 140 μV K^{-1} [47] (compare to 30 μV K^{-1} for $Y_3Ir_4Ge_{13}$), depending on the method of synthesis.

5. Conclusion

A number of temperature- and field-dependent physical properties are reported in this work on the new cubic compound $Y_3Ir_4Ge_{13}$. The compound could be classified as an intermetallic system on the edge of metallic behaviour. Interesting features that have been identified in the thermal behaviour of $Y_3Ir_4Ge_{13}$ warrant further investigation in order to categorize especially its thermoelectric properties among those of related materials of current interest, with a view on exploiting features of this structure type and elemental composition. The thermal properties found in $Y_3Ir_4Ge_{13}$ are considered to forward this structure type as an interesting alternative field of study to the presently intensively investigated materials of thermoelectric merit such as filled clathrates and skutterudites.

Measurements on single crystals are highly desirable in order to assess the importance of e.g. phase translational coherence in the electrical transport, crystalline anisotropy in the electrical and thermal transport, and the degree to which transverse/longitudinal magnetic fields might influence the transport properties of $Y_3Ir_4Ge_{13}$. High-resolution structural measurements such as x-ray or neutron diffraction are needed to clarify the nature of anharmonicity of lattice vibrations in $Y_3Ir_4Ge_{13}$.

Acknowledgments

The South African National Research Foundation, through grant GUN-2072956, and the University of Johannesburg Research Committee are thanked for financial support. R Buker is thanked for fabricating quartz ampoules for heat treatment of the samples, and N Koch is thanked for assistance in sample preparation procedures. It is a pleasure to thank Silke Bühler-Paschen and Kamran Behnia for helpful discussions.

References

[1] Remeika J P *et al* 1980 *Solid State Commun.* **34** 923
[2] Venturini G, Méot-Meyer M, Malaman B and Roques B 1985 *J. Less-Common Met.* **113** 197
[3] Miraglia S, Hodeau J L, Marezio M, Laviron C, Ghedira M and Espinosa G M 1986 *J. Solid State Chem.* **63** 358
[4] Aoki Y, Sato H, Fukuhara T, Takayanagi S, Ōnuki Y and Wada N 1993 *Physica* B **186–188** 738–40
[5] Hundley M F, Sarrao J L, Thompson J D, Movshovich R, Jaime M, Petrovic C and Fisk Z 2004 *Phys. Rev.* B **65** 24401
[6] Andres K, Remeika J P, Espinosa G P and Cooper A S 1981 *Phys. Rev.* B **23** 1179
[7] Sarkar S *et al* 2000 *Physica* C **341–348** 1055–6
[8] Sarkar S *et al* 2000 *Physica* C **341–348** 1085–6
[9] Ghosh K, Ramakrishnan S and Chandra G 1993 *Phys. Rev.* B **48** 10435
[10] Sato H, Fukuhara T, Iwakawa S, Aoki Y, Sakamoto I, Takayanagi S and Wada N 1993 *Physica* B **186–188** 630–2

[11] Nagoshi C, Sugawara H, Aoki Y, Sakai S, Kohgi M, Sato H, Onimaru T and Sakakibara T 2005 *Physica* B **359–361** 248–50
[12] Cornelius A L, Christianson A D, Lawrence J L, Fritsch V, Bauer E D, Sarrao J L, Thompson J D and Pagliuso P G 2006 *Physica* B **378–380** 113–4
[13] Israel C *et al* 2006 *Physica* B **359–361** 251
[14] Ghosh K, Ramakrishnan S, Dhar S K, Malik S K, Chandra G, Pecharsky V K, Gschneidner K A Jr, Hu Z and Yelon W B 1995 *Phys. Rev.* B **52** 7267
[15] Thomas E L, Lee H O, Bankston A N, MaQuilon S, Klavins P, Moldovan M, Young D P, Fisk Z and Chan J Y 2006 *J. Solid State Chem.* **179** 1642–9
[16] Hodeau J L, Marezio M, Remeika J P and Chen C H 1982 *Solid State Commun.* **42** 97
[17] Niepmann D, Pöttgen R, Poduska K M, DiSalvo F J, Trill H and Mosel B D 2001 *Z. Naturf.* **56b** 1
[18] Hodeau J L, Chenavas J, Marezio M and Remeika J P 1980 *Solid State Commun.* **36** 839
[19] Bordet P, Cox D E, Espinosa G P, Hodeau J L and Marezio M 1991 *Solid State Commun.* **78** 359
[20] Thomas E L, Millican J N, Okudzeto E K and Chan J Y 2006 *Comm. Inorg. Chem.* **27** 1–39
[21] Paschen S 2006 *Thermoelectric Aspects of Strongly Correlated Electron Systems* vol 1 (Boca Raton, FL: CRC Press) chapter 15, pp 1–20
[22] Venturini G, Ijjaali I and Malaman B 1999 *J. Alloys Compounds* **289** 116
[23] Jouanneaux A 1999 *CPD Newslett.* **289** 116
[24] Lawless W N 1976 *Phys. Rev.* B **14** 134
[25] Bharathi A, Mani A, Narashima Rao G V, Sundar C S and Harihan Y 1997 *Physica* B **240** 1
[26] Troć R, Strydom A M, du Plessis P de V, Tran V H, Czopnik A and Cockroft J K 2003 *Phil. Mag.* B **83** 1235
[27] Abrikosov A A 2003 *J. Phys. A: Math. Gen.* **36** 9119
[28] Stinson M R 1980 *J. Phys. F: Met. Phys.* **10** L133
[29] Lee M, Rosenbaum T F, Saboungi M L and Schnyders H S 2002 *Phys. Rev. Lett.* **88** 066602
[30] Abrikosov A A 1998 *Phys. Rev.* B **58** 2788
[31] Reale C 1973 *Appl. Phys.* **2** 183
[32] Reale C 1971 *J. Mater. Sci.* **6** 33
[33] Kittel C 1996 *Introduction to Solid State Physics* (New York: Wiley)
[34] Berman R 1978 *Thermal Conduction in Solids* (Oxford: Clarendon)
[35] Nolas G S, Weakley T J R, Cohn J L and Sharma R 2000 *Phys. Rev.* B **61** 3845
[36] Nolas G S, Morelli D T and Tritt T M 1999 *Annu. Rev. Mater. Sci.* **29** 89
[37] Paschen S, Carillo-Cabrera W, Bentien A, Tran V H, Baenitz M, Grin Yu and Steglich F 2001 *Phys. Rev.* B **64** 214404
[38] Paschen S, Pacheco V, Bentien A, Sanchez A, Carillo-Cabrera W, Baenitz M, Iversen B B, Grin Yu and Steglich F 2003 *Physica* B **328** 39
[39] Sales B C, Mandrus D and Williams R K 1996 *Science* **272** 1325–8
[40] Tritt T M 1999 *Science* **283** 804
[41] Keppens V, Mandrus D, Sales B C, Chakoumakos B C, Dai P, Coldea R, Maple M B, Gajewski D A, Freeman E J and Bennington S 1998 *Nature* **395** 876
[42] Sales B C 2002 *Science* **295** 1248–9
[43] Elliot S R 1998 *The Physics and Chemistry of Solids* (New York: Wiley)
[44] Behnia K, Jaccard D and Flouquet J 2004 *J. Phys.: Condens. Matter* **16** 5187–98
[45] Ziman J M 1972 *Principles of the Theory of Solids* (Cambridge: Cambridge University Press)
[46] Snyder G J, Christensen M, Nishibori E, Caillat T and Iversen B B 2004 *Nat. Mater.* **3** 458–63
[47] Souma T, Nakamoto G and Kurisu M 2002 *J. Alloys Compounds* **340** 275–80